Research Article Vol. 9, No. 9 / September 2022 / Optica 971

Exceptional points with memory in a microcavity Brillouin laser

Yao Chen,[1] Fangxing Zhang,[1,2] Tian Qin,[1] Guolin Zhao,[3] Jiankun Hou,[1] Xianfeng Chen,[3] Li Ge,[4,5] and Wenjie Wan[1,3,*]

[1]The State Key Laboratory of Advanced Optical Communication Systems and Networks, University of Michigan-Shanghai Jiao Tong University Joint Institute, Shanghai Jiao Tong University, Shanghai 200240, China
[2]Current address: Peking University Yangtze Delta Institute of Optoelectronics, Nantong 226010, China
[3]Department of Physics and Astronomy, Shanghai Jiao Tong University, Shanghai 200240, China
[4]Department of Physics and Astronomy, College of Staten Island, The City University of New York, New York, New York 10314, the Graduate Center, CUNY, New York, New York 10016, USA
[5]e-mail: li.ge@csi.cuny.edu
*Corresponding author: wenjie.wan@sjtu.edu.cn

Received 28 February 2022; revised 11 May 2022; accepted 26 July 2022; published 23 August 2022

Exceptional points (EPs), universally present in non-Hermitian systems, often reveal some critical behaviors such as topological encircling chirality and ultrahigh enhanced sensing near such singularities. However, most of the experimental realizations of EPs have been limited to the linear regime, where system nonlinearity has been omitted. Here, we experimentally observe two distinct EPs with opposite hermiticities and demonstrate a parity–time phase transition with exotic memory effects near the EPs in a nonlinear and non-Hermitian system based on a stimulated Brillouin laser in an optical microcavity. The self-phase modulation induced nonlinearity effectively alters the EP location, surprisingly, in an asymmetric manner, resulting in a bistable memory effect. Moreover, two EPs with opposite hermiticities in the same system are found to show quite distinct behaviors in such a memory effect. This scheme completes the studies of non-Hermitian physics in a more general scenario by including nonlinearity and paves the way toward optical memory for all-optical signal processing and quantum information.

https://doi.org/10.1364/OPTICA.456977

1. INTRODUCTION

Observables in closed physical systems are commonly associated with quantum theories and Hermitian Hamiltonians. However, a wide range of physical systems exchange particles and energy with their environment, rendering them non-Hermitian [1–3]. Despite the lack of Hermiticity, these non-Hermitian systems can display a plethora of unusual symmetries, such as parity-time (PT) symmetry, that may lead to a counterintuitive real energy spectrum [4], revealing many intriguing phenomena such as PT-symmetry breaking [5,6], pump-induced laser terminations [7], and loss-induced transparency [8]. Essential to these findings is a prominent degeneracy called an exceptional point (EP) [9,10], which marks the transition singularity between two distinct phases. An intriguing property of the EP is its strong response to external perturbations, enabling a hypersensitive sensing scheme for nanoparticles [11], lasing control [12], and optical gyroscopes [13–15]. Recently, there has been a growing interest in the dynamics near an EP, where the state evolution encircling an EP is found to be topological and chiral [16]. Moreover, non-adiabatic transitions are observed to have such chiral behaviors in non-Hermitian systems [17], leading to the demonstrations of asymmetric mode switching [16,18,19], topological energy transfer [20], and an optical omni-polarizer [21]. These captivating features show great potential for quantum control and information processing, and are universal for sound, light, microwaves, and matter wave systems [22].

Previous studies of non-Hermitian systems and their EPs focus mainly on the linear regime, where the gain and loss are assumed to be independent of the field amplitudes. However, nonlinearity does manifest itself in many non-Hermitian systems [23,24]. For example, the non-reciprocal transmission of light in coupled PT-symmetric microcavities has been attributed to the nonlinear saturation effect [25,26]. More importantly, nonlinearity, e.g., the Kerr effect, can be utilized as an additional parameter and enrich the physics near an EP [27]. Theoretical proposals have suggested the possibility of realizing an optical limiter with nonlinear instability near an EP [28]. Anomalous nonlinear PT transitions have also been proposed, including a route to the PT-broken phase away from an EP [29] and the reversal of PT transitions [30,31]. In addition, nonlinear bistability is important for topological and chiral behavior around an EP [32]. So far, these works have been limited to theoretical studies, and experiments to understand the EP with nonlinearity are critically important for applications associated with EPs in sensing and laser controlling.

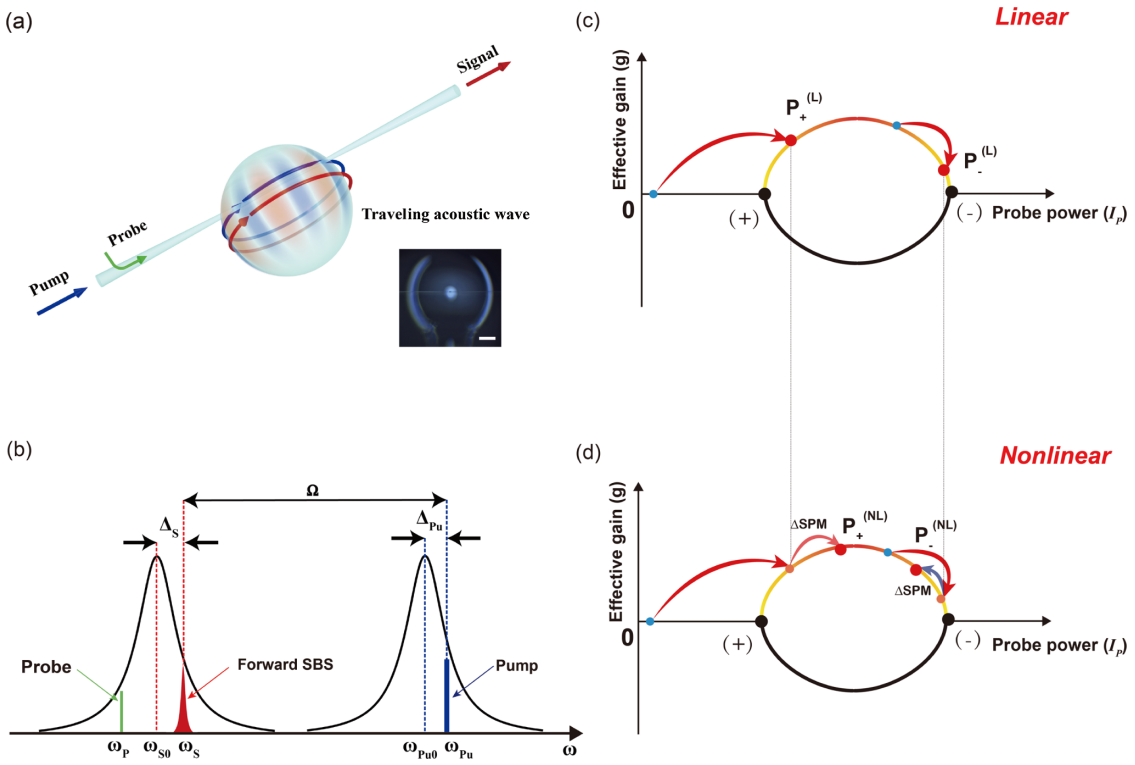

Fig. 1. Nonlinear EP in photon–phonon coupled PT-symmetry in a microcavity. (a) A forward SBS laser in a WGM microcavity consists of two optical modes, i.e., pump and Stokes, and an acoustic mode. Inset: high-Q microsphere microcavity coupled to a tapered fiber; scale bar = 50 μm. (b) Optical resonances associated with the SBS laser near the pump and Stokes modes, separated by acoustical frequency Ω. (c), (d) EPs ("+EP" and "−EP") in the effective gain curves when varying the probe's power, derived from the eigenvalues of the photon–phonon coupled Hamiltonian: (c) linear regime; (d) with nonlinearity, the increase of the probe power contracts the gain curve at +EP, but dilates it at −EP with respect to probe power.

In this work, we reveal experimentally an unusual memory effect across an EP in a nonlinear optical system: contrary to the situation in a linear system, our system may or may not return to its original PT-symmetric phase once the perturbation is removed, depending on how far the system has moved away from the EP in the PT-broken phase. We attribute this observation to nonlinearity-induced asymmetric dilation or contraction, i.e., optical nonlinearity effectively boosts or suppresses a tuning parameter that is swept across an EP. We identify three distinct scenarios, where the parametric dilation and contraction are absent, symmetric, and asymmetric. In the last case, we reveal that a system originally in the PT-symmetric phase experiences a permanent PT transition, i.e., it remains in the PT-broken phase even after the symmetry-preserving perturbation is removed. More surprisingly, we have observed two distinct EPs with opposite hermiticities in our system. We further show that the hermiticity of the EP can flip the dynamics between dilation and contraction.

2. THEORY

Such a PT transition near a nonlinear EP can be implemented using a forward-type stimulated Brillouin scattering (SBS) laser in an optical microsphere cavity [33] as in Fig. 1. Two optical modes in the microsphere are coupled through a spatially overlapping acoustic mode in this process, all of which are of whispering gallery mode [WGM, Fig. 1(b)] [34,35]. An optical pump injects intense light into the microsphere via an evanescently coupled tapered fiber, and when the phase-matching condition is satisfied, a pump photon is downconverted into a pair of acoustic phonon and Stokes photon at a lower frequency through electrostriction [35]. As we shall show below, such a system exhibits an effective PT symmetry in a photon–phonon coupled system [36], and it experiences a PT transition once the SBS laser is brought above its threshold [Fig. 1(c)]. Previously, the PT transition near an EP was proven to be highly sensitive to some external perturbations in the linear regime [11,12], which prevents the observation of delicate nonlinear effects during the transition. To mitigate this issue, here we introduce a secondary probe that co-propagates with the pump in the fiber to finely tune the PT system near its EP through nonlinear cross-phase modulation (XPM) [37–39]. In this manner, this transition can be conveniently and precisely controlled by the amplitude of the weak probe.

Quantitatively, the couplings of the pump, the Stokes, and the acoustic wave (u) inside the microsphere are typically described by the following equations ([36,40], Supplement 1, S1b):

$$H\begin{pmatrix} A_S \\ u^* \end{pmatrix} \equiv i\frac{d}{dt}\begin{pmatrix} A_S \\ u^* \end{pmatrix} = \begin{pmatrix} \Delta_S - i\kappa & \beta^* A_{Pu} \\ -\beta A_{Pu}^* & -\Delta_B - i\Gamma \end{pmatrix}\begin{pmatrix} A_S \\ u^* \end{pmatrix}. \tag{1}$$

Here, $\Delta_{Pu,S,B}$ are the frequency detunings from their cavity modes for the pump, the Stokes, and the acoustic resonance modes, respectively [Fig. 1(b)]. κ, Γ are the decay rates for optical and acoustical modes, respectively. Note that H so defined is a *linear* Hamiltonian, because it does not depend on A_S or u. Its two complex eigenvalues, i.e.,

$$\lambda_\pm = \frac{1}{2}(\Delta_S - \Delta_B - i\kappa - i\Gamma) \pm \frac{1}{2}\sqrt{\delta^2 - 4|\beta A_{Pu}|^2}, \tag{2}$$

indicate the extistance of two EPs at $\delta = \Delta_S + \Delta_B = \pm 2|\beta A_{Pu}|$, where δ measured in our experiment is up to 100 MHz, much larger than κ (∼1 MHz) and Γ (∼10 kHz); hence, κ and Γ are ignored in this approximation. The eigenvalue physically could be measured through the resonance mode and its associated linewidth in prior work [10]. Here, we focus on the one with the "+ sign. Clearly, $\lambda_\pm + \frac{i}{2}(\kappa + \Gamma)$ are real when $\delta > 2|\beta A_{Pu}|$, which is our PT-symmetric phase; $\lambda_\pm + \frac{i}{2}(\kappa + \Gamma)$ are complex conjugates when $0 < \delta < 2|\beta A_{Pu}|$, and the system is in the PT-broken phase with an effective gain factor. Note that while the time-reversal operator T still takes the familiar form of a complex conjugation [1], the parity operator is now parametrized by δ and $\beta^* A_{Pu}$ (Supplement 1, S1d). More importantly, it is crucial to note that two additional optical nonlinearities are neglected in H above; they are given by the XPM and self-phase modulation (SPM) [37–39], the dominant effect of which is to introduce small perturbations to the total detuning δ in our experiments:

$$\delta \to \delta' = \Delta_S + \Delta_B - \underbrace{2\gamma|A_{Pu}|^2 - 2\gamma|A_P|^2}_{\text{XPM}} - \underbrace{\gamma|A_S|^2}_{\text{SPM}}$$

$$\equiv \Delta_S + \Delta_B - 2\gamma I_{Pu} - 2\gamma I_P - \gamma I_S. \tag{3}$$

Here, γ is a nonlinear coefficient, A_P is the amplitude of the secondary seeded probe, and $I_{Pu,P,S}$ are the intensity terms for the pump, probe, and Stokes waves, respectively. These perturbations are inconsequential when the linear δ is tuned over a wide range across the EP, but they are extremely important when we probe the vicinity of the EP to investigate its hypersensitivity to a minute perturbation. With these additional frequency shifts and δ replaced by δ', the effective Hamiltonian H now becomes *nonlinear* due to the presence of $|A_S|^2 = I_S$. It still has two distinct phases across its EP at $\delta' = 2|\beta A_{Pu}|$, and one needs to pay special attention to the self-interaction SPM term γI_S in δ': it is nonzero only when the SBS laser is above its lasing threshold, which requires the system to be in the laser on-state (also referred as PT-broken phase in Ref. [36]).

When crossing the EPs, such nonlinearity can greatly alter the lasing dynamics, also highly depending on the hermiticity, i.e., the sign of EPs "+" or "−" ($\delta' = \pm 2\beta A_{Pu}$). For example, when exerting the same amount of external perturbation, e.g., I_P, the system can undergo a transition to an SBS laser on-state from an off-state near +EP, and quite conversely switch to a laser off-state from a laser on-state near −EP [Fig. 1(c)]. To elaborate on this transition, we first focus on the situation when crossing a "+EP." For a linear transition near an EP [Fig. 1(c)], the initial laser in off-state P_0 (with $I_{P0} = I_{S0} = 0$ for the Stokes and $\delta' = \delta'_0 > 2|\beta A_{Pu}|$) can undergo an adiabatic transition across the EP to reach lasing state $P_1^{(L)}$ (with $I_{S1} > 0$ and $\delta' = \delta'_1 < 2|\beta A_{Pu}|$) when tuning up the probe from $I_{P0} = 0$ to $I_{P1} > I_P^{(\mathrm{EP})}$. Here, $I_P^{(\mathrm{EP})} \equiv (\delta'_0/2 - |\beta A_{Pu}|)/\gamma$ is the intensity of the probe at the EP when increasing the probe, and the EP effectively marks the lasing threshold point when κ, Γ are small and negligible. The exact reversed path when reducing the probe intensity by the same amount, i.e., from I_{P1} to 0, leads to system restoration to the initial state [Fig. 1(c)], with the Stokes intensity $I_{S0} = 0$.

In contrast, the dynamics of crossing the +EP are quite distinct with the presentence of nonlinearity, where the SPM term in δ' becomes crucial. When increasing I_P again from $I_{P0} = 0$ to $I_{P1} > I_P^{(\mathrm{EP})}$ as in the linear case, the system moves further into the PT-broken phase (laser-on state) and reaches a new state $P_1^{(NL)}$ due to the SPM term γI_{S1} in δ', and the final detuning is given by $\delta'_1 = \delta'_0 - 2\gamma I_{P1} - \gamma I_{S1}$. In other words, when the PT-breaking curves (effective gain curves) are plotted using the control parameter I_P, the system effectively experiences a *contraction*: it would require increasing the control parameter I_P by $I_{P1} + I_{S1}/2$, instead of just I_{P1}, to reach state $P_1^{(NL)}$ in the linear case. This nonlinearity-induced contraction takes place only when the final state is in the PT-broken phase, and the contraction factor C can then be defined using ΔI_S and ΔI_P, i.e., the changes of I_P and I_S:

$$C = 1 + \frac{\Delta I_S}{2\Delta I_P}. \tag{4}$$

Importantly, the system can be *irreversible* when reducing I_P by the same amount back to the initial point, depending on how deep state $P_1^{(NL)}$ is in the PT-broken phase: *If* the change of δ' by just $2\gamma I_{P1}$ is not enough to go back across the EP, i.e., $\delta'_1 + 2\gamma I_{P1} < 2|\beta A_{Pu}|$, then the reduction of I_P back to zero will *not* restore the system to the PT-symmetric phase (laser-off state); it will end in state P_2 still in the PT-broken phase with the Stokes wave intensity I_{S2} [Fig. 1(e)]. In other words, this *irreversible* scenario requires $I_{S1} > (\delta'_0 - 2|\beta A_{Pu}|)/\gamma = 2I_P^{(\mathrm{EP})}$, which defines quantitatively how deep state $P_1^{(NL)}$ needs to be in the PT-broken phase. With final state P_2 still in the PT-broken phase at $I_P = 0$, this phenomenon can be interpreted as a *memory effect* [41,42]: the system remembers where it has been penetrated in the PT-broken phase [27]. Such a memory effect is universal among nonlinear systems, e.g., a nonlinear optical microcavity with stochastic resonances [43]; a similar nonlinear hysteresis response can also be found in prior works [42]. Note that such irreversibility is inherently caused by nonlinearity, not directly related to the chirality during the encircling of an EP in prior works [44], which is a purely linear system.

We first verify these expectations using temporal simulations of this nonlinear system near its EP. As shown in Fig. 2, three typical crossing scenarios are illustrated during an adiabatic tuning of I_P. In the first case [*linear regime*; Fig. 2(d)], the increment of I_P is less than its value required to reach the EP to initiate the SBS laser, i.e., $I_{P1} < I_P^{(\mathrm{EP})}$. Therefore, the temporal evolution of the Stokes depicts a flat curve in both forward and backward directions. The second case [*reversible nonlinear regime*; Fig. 2(e)] shows that the increment of I_P is large enough to elevate the system across the EP, triggering an SBS laser. The shorter arrow in the gain diagram shows the additional jump to the effective detuning δ' due to the SPM term. In the backward direction, since the reduction of I_P (back to zero) is large enough to retract the system below the laser threshold, it eliminates SBS lasing along with its SPM. This behavior leads to the reversible scenario. In the third scenario [*irreversible nonlinear regime*; Fig. 2(f)], the SBS laser also turns on when gradually increasing I_P by a large amount. The resulting large SPM satisfies the aforementioned criterion $I_{S1} > (\delta'_0 - 2|\beta A_{Pu}|)/\gamma$ and causes the system to remain in the PT-broken phase even when reducing I_P back to zero, observed from the simulated temporal evolution. Note that, unlike prior works on the encircling EP problem [16,18,19], which depends on two physical parameters to encircle around two-dimensional topological space, here only one perturbation is sufficient to cross the EP and observe such a bistable memory effect.

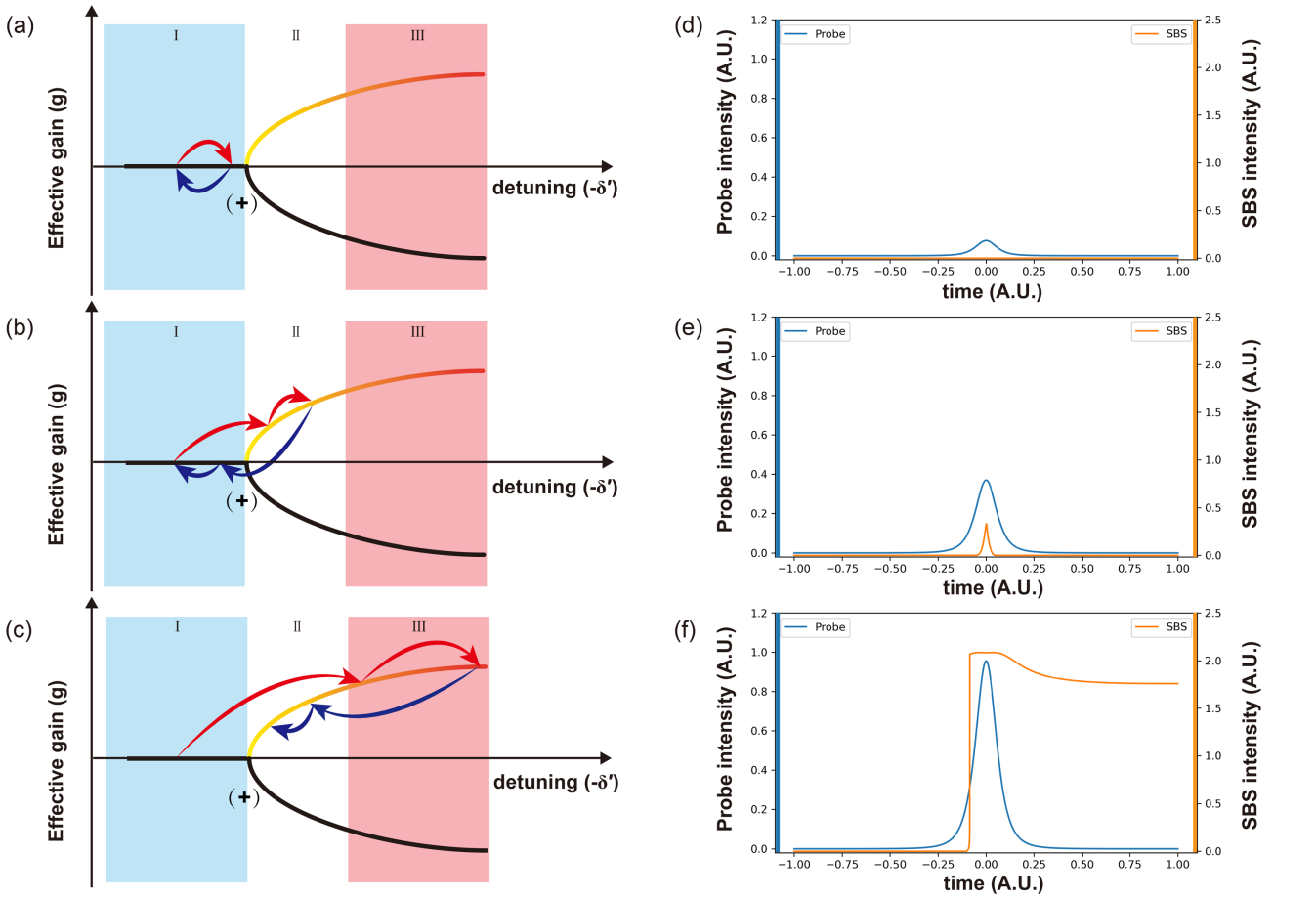

Fig. 2. Dynamics of crossing a nonlinear +EP in a gain curve with detuning. The one-dimensional encircling of an EP consists of a forward increase and a backward decrease of the detuning. (a) The crossing step (big arrows) from the external variation, e.g., the probe, is small within the PT-symmetry phase (I, linear regime), not enough to cross the EP, and the encirclement returns to its initial point without SBS lasing shown in the numerical temporal evolution (d). (b) The crossing step becomes large enough to cross the EP, initiating an SBS laser. The SPM nonlinearity (small arrows) of the laser further boosts its gain in the PT-broken phase (II, quasi-linear regime). However, the reversed path still returns to the initial point, exhibiting a laser spike during the temporal evolution (e). (c) The crossing step is sufficiently large to bring the system deep into the PT-broken phase (III, nonlinear regime), where the laser's self-induced nonlinearity can sustain the laser even after removing the external perturbation, not returning to the original point. As a result, asymmetric crossing evolution is observed in (f).

3. EXCEPTIONAL POINTS WITH MEMORY

Experimentally, we use a tapered fiber coupled WGM microsphere resonator of diameter ∼200 μm and Q-factor ∼10^7 in Fig. 3. When a strong pump is launched into the microsphere, it will excite an optical WGM, and a forward acoustic phonon will be generated that can scatter the pump beam into another optical WGM (forward Stokes photon) through an SBS process by the electrostriction effect [1,2]. The optical and acoustic WGMs can both be supported and enhanced by a microsphere cavity above the threshold if the frequency difference of the two optical WGMs matches exactly with the acoustic frequency (Supplement 1, Fig. S1). The beating frequency spectrum of the Stokes wave in Fig. 3(c) reveals a linewidth around 2.9 kHz, corresponding to a mechanical Q-factor ∼10^4. In this manner, the system contains two optical photon modes coupled by a forward acoustic phonon. To demonstrate the memory effect near a nonlinear EP, we change the pump laser detuning to tune the system near an SBS lasing threshold.

Once the system is near an SBS lasing threshold, the frequency of the probe laser will be modulated by the acoustic-optical modulator (AOM) and electrical-optical modulator (EOM) to locate near the SBS central frequency (Supplement 1, S4). The probe laser's basic intensity and frequency can be controlled precisely by the EOM with a microwave to scan across the SBS laser. During the scanning process, the probe laser will experience a Lorentz-like amplification in the SBS optical gain region [45], which is used as a natural perturbation to introduce an increasing perturbation through XPM in the forward direction and an equal decreasing perturbation in the backward direction. In other words, the term $2\gamma I_p$ in Eq. (3) will be perturbated. The time evolution spectrum of the SBS laser in Fig. 3(b) is monitored by real-time spectrum analyzer (RSA). The system can be tuned through the pump's detuning to study nonlinear behaviors at both "+" and "−" EPs.

In our experiment, we demonstrate such a memory effect near a nonlinear EP near an SBS lasing threshold as in Fig. 3. Our system is prepared to operate slightly *below its SBS lasing threshold* by controlling the pump's detuning frequency Δ_{Pu} (∼10 MHz) and power I_{Pu} (∼5 mW). Near this threshold, lasers are extremely sensitive [11,12,14,15]; hence, we find that the XPM from a probe can be utilized as a precise and non-disturbing tool to control the laser. Here, instead of changing the probe intensity directly, we keep the power of the probe fixed but sweep its frequency near the

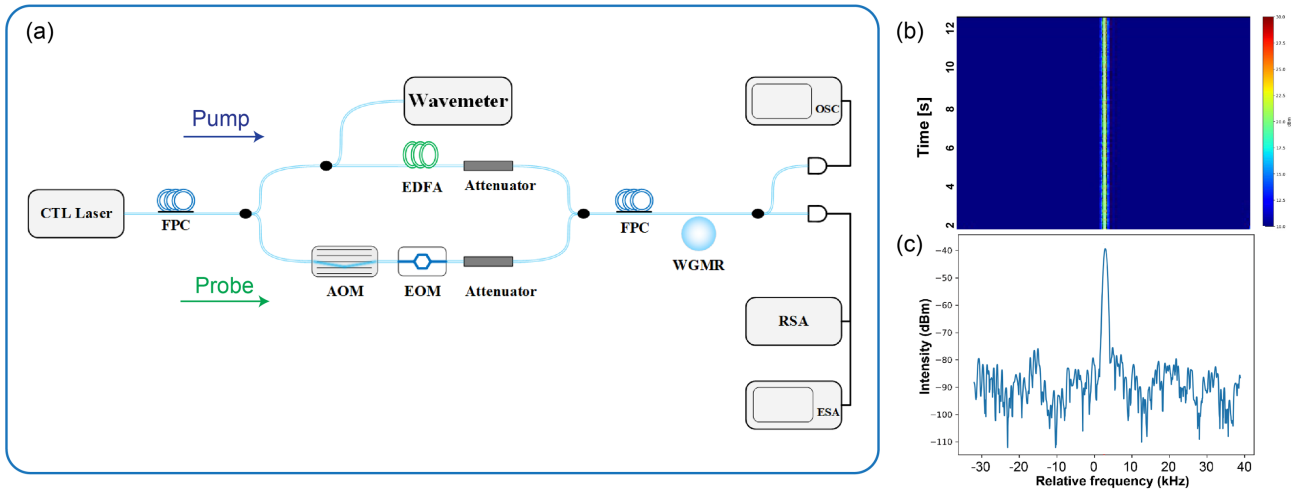

Fig. 3. Experimental setup of optical memory effect of an SBS laser. (a) Schematic illustration of the experimental setup to realize optical memory effect based on Brillouin laser in a microsphere cavity. The upper optical path is the pump laser; the wavemeter is used to monitor the current wavelength of the pump. The lower optical path is the probe laser modulated to scan across the SBS laser through an electrical-optical modulator (EOM). The acoustic-optical modulator is used to help distinguish between Stokes and anti-Stokes. Time evolution spectrum of SBS laser during probe scanning is recorded by RSA, and the beat frequency spectrum is recorded by an electrical spectrum analyzer (ESA) (b) Two-dimensional spectra of a static SBS laser in frequency (horizontal axis) with time evolution (vertical axis); note that the probe is absent in this case. (c) Beating frequency spectrum of an SBS laser in an electrical spectrum analyzer.

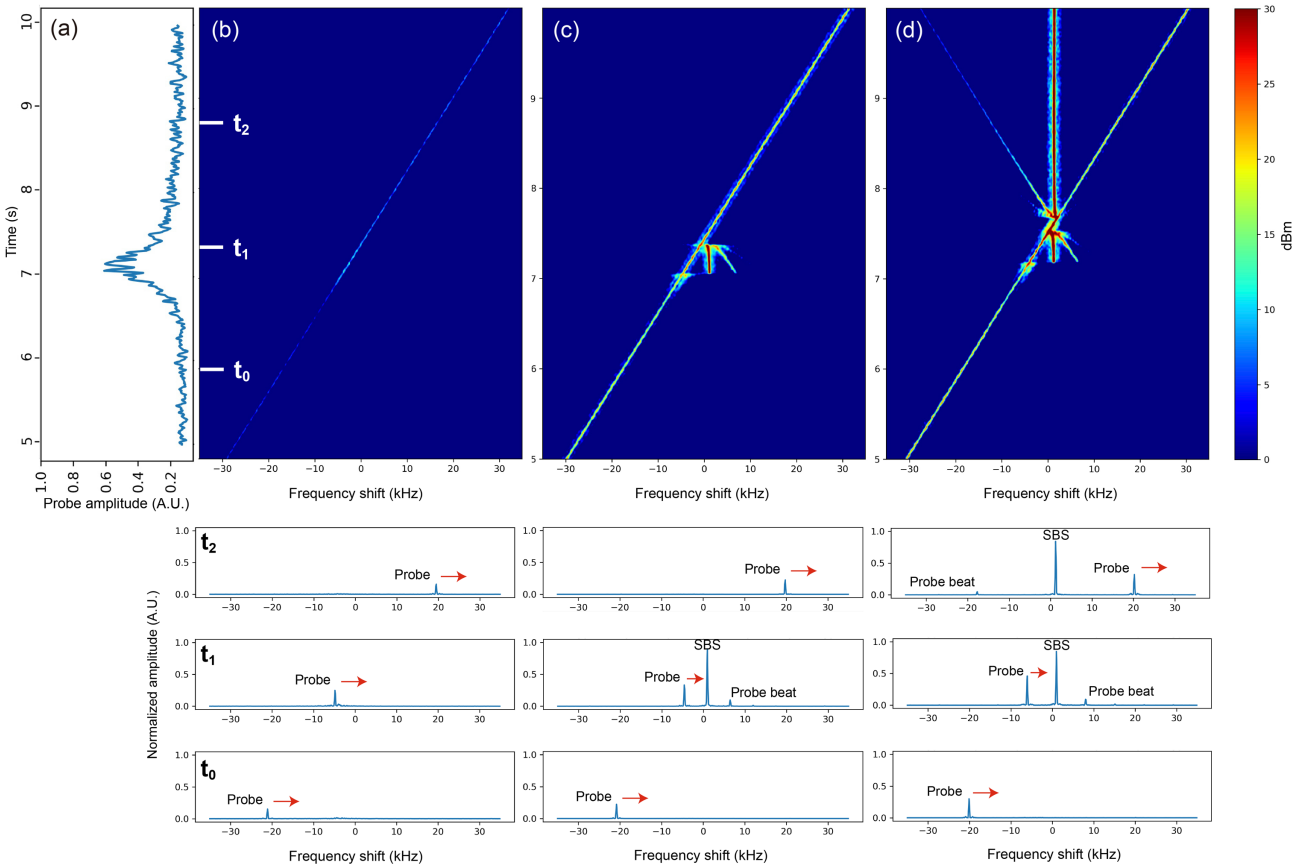

Fig. 4. Experimental observation of optical memory effect of an SBS laser when crossing a nonlinear +EP. (a) The temporal evolution of the probe's amplitude when scanning through the Stokes resonance gives rise to a spike due to the resonance enhancement. (b)–(d) Two-dimensional spectra in frequency (horizontal axis) during the probe's scan (vertical axis). (b) The probe's power is controlled at around 65.83 μW. No SBS laser is observed in the selected spectrum shown at three typical time slots, t_0, t_1, and t_2. The crossing step is small within the PT-symmetric phase (I, linear regime), not enough to cross the +EP; (c) increasing the probe power to 202.66 μW, an SBS laser is clearly visible at t_1 but disappears again at t_2 when reducing the probe's power. (d) Further increase of the probe power to 388.31 μW leads to a self-sustained lasing action at t_2, even after removing the probe.

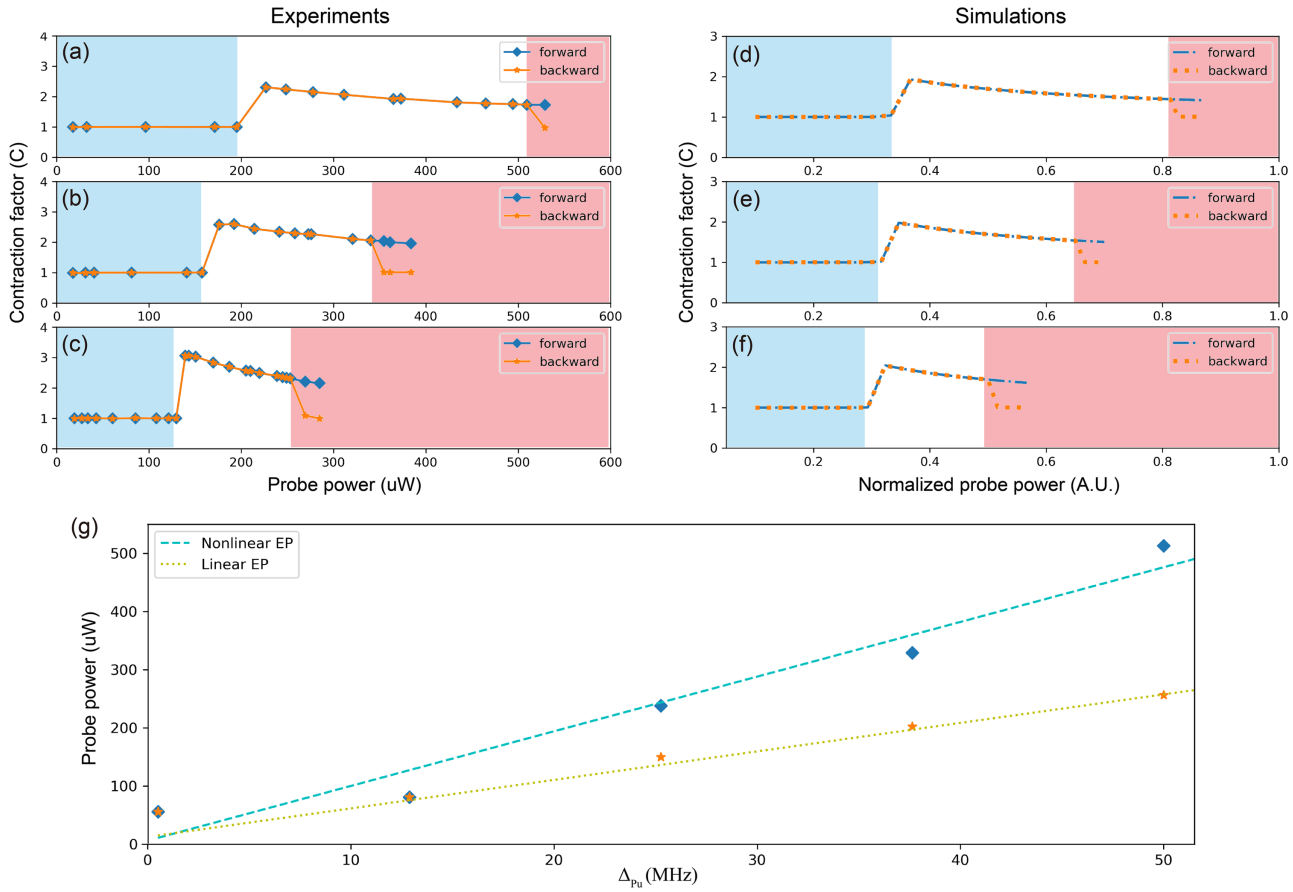

Fig. 5. Phase transitions near the nonlinear +EP. (a)–(f) Contraction factors of the forward and backward crossing of the +EP when tuning the probe's power at different initial detuning points, i.e., (a) 50 MHz, (b) 38 MHz, and (c) 25 MHz. (a)–(c) Experimental results; (d)–(f) numerical simulations. The first phase transitions during tuning up the probe's power occur around the EP, i.e., $\delta' = 2\beta A_{Pu}$, and the forward and backward contraction factors still coincide, i.e., $C_{\text{Forward}} = C_{\text{Backward}}$. On the other hand, the divergence of C_{Forward}, C_{Backward} indicates the second phase transition due to the presence of nonlinear SPM. The required probe's power to reach both phase transitions is plotted in (g), showing a higher threshold to reach the nonlinear bistable state than the linear EP.

Stokes resonance, where the SBS laser is supposed to be turned on. As the probe frequency approaches the SBS laser frequency, it also experiences a Brillouin gain that enhances its power [Fig. 3(a)]. Similar dynamics have been reported previously as induced transparency ([40], Supplement 1, S3). Here, the rising intracavity probe's intensity is corresponding to a forward crossing step in Fig. 2, while the decreasing one represents the backward crossing scenario. Therefore, this monotonic sweeping of the probe's frequency leads to a rise and fall of the XPM term in δ', which we find to be convenient to fine-tune the latter experiments.

Figures 4(b)–4(d) show the SBS lasing dynamics in the frequency spectrum during the probe's scanning under three representative levels of power. In each case, I_P is adiabatically tuned during the scan; three typical spectra when the probe is at the starting point (I_P is small), reentry point (I_P is at the peak), and ending point (I_P becomes small again) are depicted to show the corresponding laser signals. In the first case [*linear regime*; Fig. 4(b)], the increase is less than the value required to reach the EP to initiate the SBS laser, i.e., $I_{P1} < I_P^{(\text{EP})}$. Therefore, the temporal evolution of the Stokes depicts a flat curve in both forward and backward directions. The second case [*reversible nonlinear regime*; Fig. 4(c)] shows that the increase of I_P is large enough to elevate the system across the EP, triggering an SBS laser. In the backward direction, since the reduction of I_P (back to zero) is large enough to retract the system below the laser threshold, it eliminates SBS lasing along with its SPM. This behavior leads to a reversible scenario. In the third scenario [*irreversible nonlinear regime*; Fig. 4(d)], the SBS laser also turns on when gradually increasing I_P by a large amount. The resulting large SPM satisfies the aforementioned criterion $I_{S1} > (\delta_0' - 2|\beta A_{Pu}|)/\gamma$ and causes the system to remain in the PT-broken phase even when reducing I_P back to zero, i.e., laser memory effect [41]. Similar nonlinear hysteresis curves can also be obtained by tracing the SBS intensity with respect to the varying probe; more details are shown in Supplement 1. Note that the probe beam can intermix with the SBS laser signal near the gain center in Fig. 4(d), due to the nonlinear locking mechanism [14].

To better characterize this memory effect near a nonlinear EP, we experimentally measure the contraction factor C for the two pathways: the forward path when tuning I_P from the starting point to the reentry point, and the backward path when tuning I_P from the reentry point to the ending point. In this manner, the recurrence of the two contraction factors, i.e., $C_{\text{Forward}} = C_{\text{Backward}}$, can reveal the linear and quasi-linear regimes; the divergence between them, i.e., $C_{\text{Forward}} \neq C_{\text{Backward}}$, indicates the occurrence of the laser bistable memory effect. As shown in Fig. 5(a), when gradually increasing the probe's power while fixing the pump's frequency and power, both C_{Forward}, C_{Backward} terms stay close to one, until the probe power reaches the threshold of ~200 μW [Fig. 5(a)].

Above this threshold, both terms synchronously jump to a higher state but are still equivalent to each other. Note that both factors are slightly declining in this state because of the laser saturation ([32,33], Supplement 1, S6). In the third stage when the probe's power reaches ~500 μW, the two terms start to diverge. Notably, C_{Backward} approaches a lower value, indicating the occurrence of the memory effect.

The three aforementioned scenarios are universal and dependent on how close the initial state is to the EP [Figs. 5(a)–5(c)]. To adjust the latter, we reduce the pump detuning Δ_{Pu} while keeping its amplitude fixed, which leads to an initial state closer to the EP with everything else unchanged. From Figs. 5(a)–5(c), the initial state is approaching the EP, i.e., reducing δ', which dramatically reduces the required probe power to reach the linear EP, i.e., $I_P^{(\text{EP})} \equiv (\delta_0'/2 - |\beta A_{Pu}|)/\gamma$. Recall that $I_{S1} > 2I_P^{(\text{EP})}$ is the condition for irreversible PT breaking. Since now a smaller probe intensity $I_P^{(\text{EP})}$ is needed to reach the EP, the onset of the irreversible process also requires a weaker intensity of the SBS laser. In other words, the range of reversible PT breaking (white region in Fig. 5) is reduced. Similar dynamics have been verified through a set of numerical results by incorporating a saturable gain model in Figs. 5(d)–5(f) (details in Supplement 1, S5). From these results, the linear and nonlinear EP conditions from the pump's detuning and the probe's power are summarized in Fig. 5(g), which depicts the linear dependences for both cases, but a higher threshold for the irreversible nonlinear PT breaking is required. Usually, these features are hard to access and hidden in most of the prior work involving PT symmetry or dynamics near EPs, due to extreme sensitivity near EPs [11,12,14,15]. Due to the current fine-tuning technique using XPM, we can reveal such a transition from a quasi-linear regime to a nonlinear one.

4. MEMORY EFFECT NEAR AN EXCEPTIONAL POINT WITH NEGATIVE HERMITICITY

Last, we experimentally demonstrate the exact opposite effect, i.e., *dilation* can occur in the crossing case of a −EP. As shown in Fig. 6, the SBS laser is initially at the PT-broken phase; however, the laser power is suppressed when increasing I_P in sharp contrast to the former "+EP" case [Fig. 6(a)]. Moreover, such power reduction leads to a "backward" retraction in the effective detuning δ' [Fig. 6(c)], i.e., *dilation*, instead of *contraction* in the +EP scenario. Like the "+EP," there also exist *reversible* and *irreversible* nonlinear regimes, in which the reversible one permits the state back to its starting point when the perturbation tuning of I_P is relatively small, i.e. $I_{S1} > (\delta_0' + 2|\beta A_{Pu}|)/\gamma$ in Fig. 6(a). Otherwise, an irreversible dynamic can be expected in Fig. 6(b),

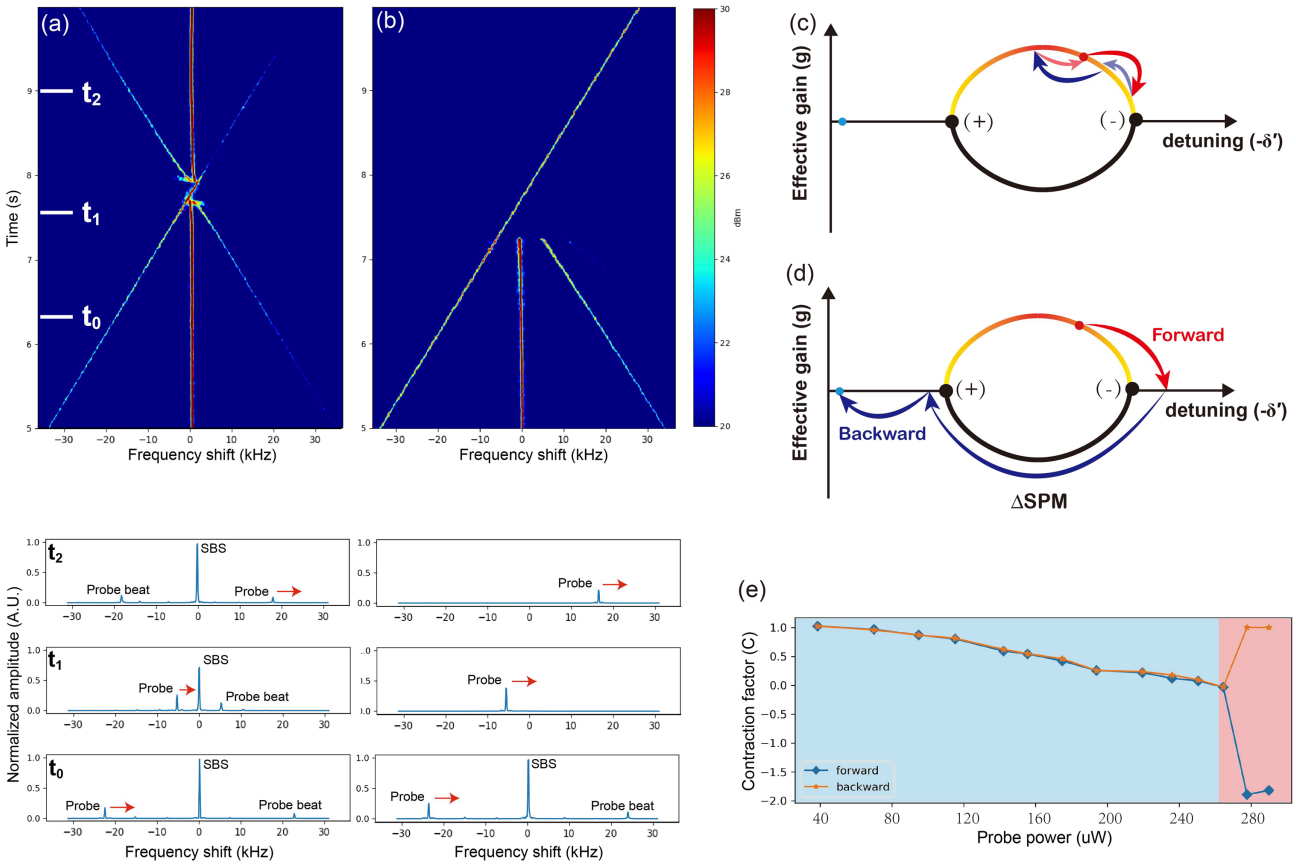

Fig. 6. Experimental observation of dilation during crossing a nonlinear −EP. (a), (b) Two-dimensional spectra in frequency (horizontal axis) during the probe's scan (vertical axis) (a); the probe's power is controlled around 120 μW. The SBS laser intensity is clearly suppressed at t_1. (c) Further increase of the probe power to around 260 μW; the SBS laser is terminated forever at t_1. (c), (d) Dynamics of crossing the −EP in a gain curve with detuning: (c) the crossing step from the weak probe is small, not enough to cross the −EP, and the encirclement returns to its initial point with SBS intensity suppressed temporarily. (d) The crossing step is large enough to cross the −EP, i.e., shutdown the SBS laser; the sudden huge intensity attenuation causes a large backward step across the opposite side near +EP due to the loss of SPM. The SBS laser will be forever shut down even after removing the external perturbation. (e) Contraction factors are below one, indicating the dilation, and the divergence point of two contraction factors shows the required probe's power to terminate the SBS laser.

where the strong I_P's tuning causes the forever shutdown of the laser. We can also distinguish these two regimes by reading out the contraction factor, i.e., C_{Forward}, C_{Backward} [Fig. 6(e)], which depicts that for a low power I_P smaller than a threshold ~260 μW, $C_{\text{Forward}} = C_{\text{Backward}}$ and both their values are below one, indicating the dilation (above one means contraction in the +EP). Again, until the threshold point, the divergence between the two terms, i.e., $C_{\text{Forward}} \neq C_{\text{Backward}}$, results in the bistable laser shutdown.

5. CONCLUSION

In summary, we experimentally demonstrated a PT transition with an unusual memory effect near an EP in a nonlinear SBS laser system. This work opens a new frontier of non-Hermitian physics into a more realistic situation by embracing nonlinearity. We would expect more intriguing effects when combining nonlinearity into the EP encircling problems in the future, especially with a high-order EP. Our results may also pave the way for practical non-Hermitian laser devices for all-optical memory and switching applications.

Funding. National Natural Science Foundation of China (92050113, 11674228, 11304201); National Key Research and Development Program of China (2016YFA0302500, 2017YFA0303700); Shanghai MEC Scientific Innovation Program (E00075).

Disclosures. The authors declare no conflicts of interest.

Data availability. The data that support the findings of this study are available from the authors upon reasonable request.

Supplemental document. See Supplement 1 for supporting content.

REFERENCES

1. L. Feng, R. El-Ganainy, and L. Ge, "Non-Hermitian photonics based on parity–time symmetry," Nat. Photonics **11**, 752–762 (2017).
2. R. El-Ganainy, K. G. Makris, M. Khajavikhan, Z. H. Musslimani, S. Rotter, and D. N. Christodoulides, "Non-Hermitian physics and PT symmetry," Nat. Phys. **14**, 11–19 (2018).
3. Ş. K. Özdemir, S. Rotter, F. Nori, and L. Yang, "Parity–time symmetry and exceptional points in photonics," Nat. Mater. **18**, 783–798 (2019).
4. C. M. Bender and S. Boettcher, "Real spectra in non-Hermitian Hamiltonians having P T symmetry," Phys. Rev. Lett. **80**, 5243 (1998).
5. A. Guo, G. J. Salamo, D. Duchesne, R. Morandotti, M. Volatier-Ravat, V. Aimez, G. A. Siviloglou, and D. N. Christodoulides, "Observation of PT-symmetry breaking in complex optical potentials," Phys. Rev. Lett. **103**, 093902 (2009).
6. C. E. Rüter, K. G. Makris, R. El-Ganainy, D. N. Christodoulides, M. Segev, and D. Kip, "Observation of parity–time symmetry in optics," Nat. Phys. **6**, 192–195 (2010).
7. M. Liertzer, L. Ge, A. Cerjan, A. Stone, H. Türeci, and S. Rotter, "Pump-induced exceptional points in lasers," Phys. Rev. Lett. **108**, 173901 (2012).
8. B. Peng, Ş. K. Özdemir, S. Rotter, H. Yilmaz, M. Liertzer, F. Monifi, C. M. Bender, F. Nori, and L. Yang, "Loss-induced suppression and revival of lasing," Science **346**, 328–332 (2014).
9. M. A. Miri and A. Alù, "Exceptional points in optics and photonics," Science **363**, 6422 (2019).
10. S. Klaiman, U. Günther, and N. Moiseyev, "Visualization of branch points in PT-symmetric waveguides," Phys. Rev. Lett. **101**, 080402 (2008).
11. W. Chen, Ş. K. Özdemir, G. Zhao, J. Wiersig, and L. Yang, "Exceptional points enhance sensing in an optical microcavity," Nature **548**, 192–196 (2017).
12. H. Hodaei, A. Hassan, S. Wittek, H. Garcia-Gracia, R. El-Ganainy, D. N. Christodoulides, and M. Khajavikhan, "Enhanced sensitivity at higher-order exceptional points," Nature **548**, 187–191 (2017).
13. J. Ren, H. Hodaei, G. Harari, A. U. Hassan, W. Chow, M. Soltani, D. Christodoulides, and M. Khajavikhan, "Ultrasensitive micro-scale parity-time-symmetric ring laser gyroscope," Opt. Lett. **42**, 1556–1559 (2017).
14. Y. H. Lai, Y. K. Lu, M. G. Suh, Z. Yuan, and K. Vahala, "Observation of the exceptional-point-enhanced Sagnac effect," Nature **576**, 65–69 (2019).
15. M. P. Hokmabadi, A. Schumer, D. N. Christodoulides, and M. Khajavikhan, "Non-Hermitian ring laser gyroscopes with enhanced Sagnac sensitivity," Nature **576**, 70–74 (2019).
16. J. Doppler, A. Mailybaev, J. Böhm, U. Kuhl, A. Girschik, F. Libisch, T. J. Milburn, P. Rabl, N. Moiseyev, and S. Rotter, "Dynamically encircling an exceptional point for asymmetric mode switching," Nature **537**, 76–79 (2016).
17. C. Wang, X. Jiang, G. Zhao, M. Zhang, C. W. Hsu, B. Peng, A. D. Stone, L. Jiang, and L. Yang, "Electromagnetically induced transparency at a chiral exceptional point," Nat. Phys. **16**, 334–340 (2020).
18. R. Uzdin, A. Mailybaev, and N. Moiseyev, "On the observability and asymmetry of adiabatic state flips generated by exceptional points," J. Phys. A Math. Theor. **44**, 435302 (2011).
19. X. L. Zhang, T. Jiang, and C. T. Chan, "Dynamically encircling an exceptional point in anti-parity-time symmetric systems: asymmetric mode switching for symmetry-broken modes," Light Sci. Appl. **8**, 88 (2019).
20. H. Xu, D. Mason, L. Jiang, and J. G. E. Harris, "Topological energy transfer in an optomechanical system with exceptional points," Nature **537**, 80–83 (2016).
21. A. U. Hassan, B. Zhen, M. Soljačić, M. Khajavikhan, and D. N. Christodoulides, "Dynamically encircling exceptional points: exact evolution and polarization state conversion," Phys. Rev. Lett. **118**, 093002 (2017).
22. C. Shi, M. Dubois, Y. Chen, H. Ramezani, Y. Wang, and X. Zhang, "Accessing the exceptional points of parity-time symmetric acoustics," Nat. Commun. **7**, 11110 (2016).
23. L. Ge and W. Wan, "Nonlinear and novel phenomena in non-Hermitian photonics," in *Emerging Frontiers in Nonlinear Science* (Springer, 2020), pp. 227–248.
24. S. Xia, D. Kaltsas, D. Song, I. Komis, J. Xu, A. Szameit, H. Buljan, K. G. Makris, and Z. Chen, "Nonlinear tuning of PT symmetry and non-Hermitian topological states," Science **372**, 72–76 (2021).
25. B. Peng, Ş. K. Özdemir, F. Lei, F. Monifi, M. Gianfreda, G. L. Long, and L. Yang, "Parity–time-symmetric whispering-gallery microcavities," Nat. Phys. **10**, 394–398 (2014).
26. L. Chang, X. Jiang, S. Hua, C. Yang, J. Wen, L. Jiang, and M. Xiao, "Parity–time symmetry and variable optical isolation in active–passive-coupled microresonators," Nat. Photonics **8**, 524–529 (2014).
27. S. Ramezanpour and A. Bogdanov, "Tuning exceptional points with Kerr nonlinearity," Phys. Rev. A **103**, 043510 (2021).
28. S. Suwunnarat, R. Kononchuk, A. Chabanov, I. Vitebskiy, N. I. Limberopoulos, and T. Kottos, "Enhanced nonlinear instabilities in photonic circuits with exceptional point degeneracies," Photon. Res. **8**, 737–744 (2020).
29. L. Ge, "Anomalous parity-time–symmetry transition away from an exceptional point," Phys. Rev. A **94**, 013837 (2016).
30. L. Ge and R. El-Ganainy, "Nonlinear modal interactions in parity-time (PT) symmetric lasers," Sci. Rep. **6**, 24889 (2016).
31. A. U. Hassan, H. Hodaei, M. A. Miri, M. Khajavikhan, and D. N. Christodoulides, "Nonlinear reversal of the PT-symmetric phase transition in a system of coupled semiconductor microring resonators," Phys. Rev. A **92**, 063807 (2015).
32. H. Wang, S. Assawaworrarit, and S. Fan, "Dynamics for encircling an exceptional point in a nonlinear non-Hermitian system," Opt. Lett. **44**, 638–641 (2019).
33. J. Yang, T. Qin, F. Zhang, X. Chen, X. Jiang, and W. Wan, "Multiphysical sensing of light, sound and microwave in a microcavity Brillouin laser," Nanophotonics **9**, 2915–2925 (2020).
34. M. Tomes and T. Carmon, "Photonic micro-electromechanical systems vibrating at X-band (11-GHz) rates," Phys. Rev. Lett. **102**, 113601 (2009).
35. G. Bahl, J. Zehnpfennig, M. Tomes, and T. Carmon, "Stimulated optomechanical excitation of surface acoustic waves in a microdevice," Nat. Commun. **2**, 403 (2011).
36. F. Zhang, Y. Feng, X. Chen, L. Ge, and W. Wan, "Synthetic anti-PT symmetry in a single microcavity," Phys. Rev. Lett. **124**, 053901 (2020).
37. Y. Zheng, T. Qin, J. Yang, X. Chen, L. Ge, and W. Wan, "Observation of gain spiking of optical frequency comb in a microcavity," Opt. Express **25**, 31140–31147 (2017).

38. Q. T. Cao, H. Wang, C.-H. Dong, H. Jing, R.-S. Liu, X. Chen, L. Ge, Q. Gong, and Y.-F. Xiao, "Experimental demonstration of spontaneous chirality in a nonlinear microresonator," Phys. Rev. Lett. **118**, 033901 (2017).
39. L. Del Bino, J. Silver, S. Stebbings, and P. Del'Haye, "Symmetry breaking of counter-propagating light in a nonlinear resonator," Sci. Rep. **7**, 43142 (2017).
40. J. H. Kim, M. C. Kuzyk, K. Han, H. Wang, and G. Bahl, "Non-reciprocal Brillouin scattering induced transparency," Nat. Phys. **11**, 275–280 (2015).
41. Z. A. Cochran, A. Saxena, and Y. N. Joglekar, "Parity-time symmetric systems with memory," Phys. Rev. Res. **3**, 013135 (2021).
42. W. Wan, S. Muenzel, and J. W. Fleischer, "Wave tunneling and hysteresis in nonlinear junctions," Phys. Rev. Lett. **104**, 073903 (2010).
43. K. J. H. Peters, Z. Geng, K. Malmir, J. M. Smith, and S. R. K. Rodriguez, "Extremely broadband stochastic resonance of light and enhanced energy harvesting enabled by memory effects in the nonlinear response," Phys. Rev. Lett. **126**, 213901 (2021).
44. L. Jin, "Parity-time-symmetric coupled asymmetric dimers," Phys. Rev. A **97**, 012121 (2018).
45. T. Qin, J. Yang, F. Zhang, Y. Chen, D. Shen, W. Liu, L. Chen, X. Jiang, X. Chen, and W. Wan, "Fast-and slow-light-enhanced light drag in a moving microcavity," Commun. Phys. **3**, 118 (2020).